Biochemical Pharmacology 80 (2010) 370–380

Contents lists available at ScienceDirect

Biochemical Pharmacology

journal homepage: www.elsevier.com/locate/biochempharm

Rimonabant-induced apoptosis in leukemia cell lines: Activation of caspase-dependent and -independent pathways

Dario Gallotta, Patrizia Nigro, Roberta Cotugno, Patrizia Gazzerro, Maurizio Bifulco, Maria Antonietta Belisario *

Dipartimento di Scienze Farmaceutiche, Università degli Studi di Salerno, Via Ponte Don Melillo, 84084 Fisciano (SA), Italy

ARTICLE INFO

Article history:
Received 8 February 2010
Accepted 16 April 2010

ABSTRACT

Rimonabant (SR141716), a cannabinoid CB1 receptor antagonist known for anti-obesity activity, has more recently been shown to inhibit tumor cell growth. Here we demonstrated the antitumor potential of SR141716 in leukemia-derived cell lines and its low toxicity in normal cells (PBMC). SR141716 (1–20 μM range of doses) reduced Jurkat and U937 cell number by activating death signals as well as affecting cell cycle progression. The most prominent response in U937 to SR141716 was a G_0/G_1 block, while in Jurkat cells there was activation of cell death processes. SR141716-treated cells exhibited the morphological and biochemical features of apoptosis and to some extent necrosis. Apoptotic mode of cell death was confirmed in both cell lines by analysis of cell morphology, phosphatidylserine exposure and DNA fragmentation. Moreover, the drug was found to induce an early and robust mitochondrial membrane depolarization. In Jurkat cells the apoptotic process was typically caspase-dependent, while in U937 caspase-independent pathways were also activated. The contribution of PARP activation to SR141716-induced apoptosis in U937 was suggested by protein PARylation, AIF release and apoptosis reversal by PARP inhibitors. Moreover, SR141716 negatively modulated, especially in U937, the PI3K/AKT pathways. In conclusion, our data indicate that SR141716 elicits alternative response and/or cell death pathways depending on the cell type affected.

1. Introduction

The term "endocannabinoid system" (ES) was coined to indicate the complex signalling system of cannabinoid receptors, endogenous ligands and the enzymes responsible for their biosynthesis and inactivation ([1,2] and references therein). Along with the endocannabinoids, the ES encompasses proteins that modulate the levels of these compounds, their biosynthetic and degradative enzymes and putative transporters, the major endocannabinoid receptors, named CB1 and CB2, and the transient receptor potential channels of the vanilloid type-1 (TRPV1).

The ubiquitous regulatory actions of the ES in health and disease emphasize its role in several physio-pathological processes and suggest distinct targets through which this signalling system could be modulated for therapeutic gain [3,4]. Increasing evidence suggests that cannabinoids exert both direct and indirect effects on cancer by different mechanisms of action in different types of malignancies [5,6]. Cannabinoids have been found to control cell growth and death in many cancer types, both in vitro and in vivo [7–9], as well as the neoangiogenesis and metastatic spreading [10–13], but the mechanisms underlying the antitumor effects are sometimes cell type specific.

Human leukemia and lymphoma cell lines, expressing CB2 and lacking CB1 receptor, were susceptible to apoptosis induced by several natural and synthetic CB receptor agonists [14]. However, in the same cells pre-treatment with SR144528 (a selective CB2 antagonist) failed to completely revert tetrahydrocannabinol (THC)-induced apoptosis, suggesting that the observed effects were not completely dependent upon this receptor. On the other hand, other reports demonstrate that cannabinoids exert their tumor cell death-promoting activity through mechanisms independent of CB receptors [15,16]. In their study, Maccarrone et al. [15] showed that Anandamide, the first endocannabinoid to be identified, induced apoptosis in the U937 cell line through the vanilloid receptor and this effect was potentiated by the inhibitors of Anandamide degradation. The apoptosis induced by Anandamide was associated with an increase in intracellular calcium, drop in mitochondrial membrane potential, release of cytochrome *c* and activation of caspases.

SR141716 (Rimonabant, Acomplia®) is the first selective cannabinoid receptor CB1 antagonist described [17]. Along with its anti-obesity action, emerging findings show potential anti-

* Corresponding author at: Dipartimento di Scienze Farmaceutiche, Università di Salerno, Via Ponte Don Melillo, 84084 Fisciano, Salerno, Italy. Tel.: +39 089 969740; fax: +39 089 969602.
E-mail address: mabelisa@unisa.it (M.A. Belisario).

0006-2952/$ – see front matter © 2010 Elsevier Inc. All rights reserved.
doi:10.1016/j.bcp.2010.04.023

proliferative and anti-inflammatory actions of SR141716 in several in vitro and in vivo models [18]. In human peripheral blood mononuclear cells (PBMC) SR141716 significantly inhibited the proliferative response to mitogens and this effect was accompanied by a G1/S phase arrest without induction of apoptosis and cell death [19]. Moreover, in this model SR141716 used in combination with 2-methylarachidonyl-2′-fluoro-ethylamide, a stable analogue of the Anandamide, showed synergism rather than antagonism of the inhibition of PBMC proliferation, indicating the multifaceted role of SR141716 in the control of cell fate. Flygare and colleagues [20] demonstrated that micromolar concentrations of SR141716 decreased viability of primary mantle cell lymphoma (MCL) isolated from human tumor biopsies. Moreover, in the MCL cell line Rec-1, combined treatment with SR141716 and Anandamide, used at equipotent doses, showed an additive effect in the inhibition of cancer cell proliferation. Synergic anti-proliferative effect of SR141716 and oxaliplatin, one of the cytotoxic drugs currently used in the treatment of colorectal cancer, was also demonstrated in human colon cancer cell line, DLD-1 [21]. Even if increasing evidence demonstrated the antitumor action of SR141716, the molecular mechanism underlying this effect is still unclear and is yet not extensively investigated [22].

In this study, we have evaluated the antitumor potential of SR141716 in two leukemia-derived cell lines, Jurkat and U937 cells. Aimed to clarify the mechanisms underlying SR141716 cell growth inhibition activity, we analyzed the effect of the drug on cell cycle progression, cell death and apoptosis. The contribution of mitochondria and caspase, PARP1, and PI3K/AKT pathways in the SR141716-induced cell death was also investigated.

2. Material and methods

2.1. Materials

Chemicals: SR141716 was kindly provided by Sanofi-Aventis (Montpellier, France). Foetal bovine serum (FBS) was from Bio-Whittaker, Hoechst 33342 and inhibitors (PJ34, ZVAD-fmk) were from Calbiochem. All the other reagents were from Sigma–Aldrich. *Antibodies*: anti-cytochrome *c* antibody (mouse mAb, 556433), anti-HSP60 (mouse, 611562) and anti-PAR (rabbit, 551813) from BD Pharmingen; anti-pAKT (Ser 473, mouse mAb, 9271), anti-AKT (rabbit, 9272) and anti-cleaved caspase 3 (Asp 175, rabbit, 9661) from Cell Signaling; anti-AIF (H-300, sc-5586), anti GAPDH (mouse mAb, sc-32233), and anti-PARP1 (mouse mAb, sc-8007) from Santa Cruz Biotechnology; anti-α tubulin (mouse mAb, T 5168) from Sigma–Aldrich; appropriate peroxidase-conjugated secondary antibodies from Jackson ImmunoResearch.

2.2. Cell culture and treatments

Jurkat and U937 cells, obtained from Cell Bank in GMP-IST (Genova, Italy), were maintained in RPMI 1640 medium supplemented with 10% (v/v) FBS, 2 mM L-glutamine and antibiotics at 37 °C in humidified atmosphere with 5% CO_2. All the experiments were performed by using cells seeded at a density of 2×10^5 cells/ml. Under given experimental conditions, untreated leukemia cells were able to double their number within less than 24 h.

SR141716 stock solutions (50 mM) in DMSO were stored at −20 °C and appropriately diluted in the same solvent or directly in the medium just before use. The final concentration of DMSO never exceeded 0.15% (v/v), a non-cytotoxic concentration, and was equal in samples and controls. Other treatments: cells were pre-incubated with Z-VAD-fmk (ZVAD) (20 μM), PJ34 (4 μM), and LY294002 (15 μM) for 2 h, or for 30 min with 500 nM 1,2-bis-(o-aminophenoxy)-ethane-*N*,*N*,*N*′,*N*′-tetra acetic acid-tetraacetoxymethyl ester (BAPTA-AM), a cell permeable Ca^{2+} chelator.

Human peripheral blood mononuclear cells (PBMC) were isolated from buffy coats of healthy donors (kindly provided by the Blood Center of the Hospital of Battipaglia, Salerno, Italy) by using standard Ficoll–Hypaque gradients. Freshly isolated PBMC contained 92.8 ± 3.1% live cells.

2.3. Cell proliferation and viability

Cells were seeded in 96-well plates (2×10^4/well) and incubated for the established times in the absence and in the presence of different concentrations of SR141716. The number of viable cells was quantified by CellTiter-Blue® Cell Viability assay (Promega) and by cytometric count (trypan blue exclusion test).

2.4. Flow cytometric and fluorometric analysis

2.4.1. Cell cycle and hypodiploidia

Cellular DNA content was evaluated by propidium iodide (PI) staining of permeabilized cells according to the available protocol [23]. Data from 10,000 to 20,000 events per sample were collected. The percentages of the elements in the hypodiploid region were calculated using the CellQuest software and those in G_0/G_1, S and G_2/M phases of the cell cycle were determined using the MODFIT software (Becton Dickinson, San Jose, CA, USA).

2.4.2. Apoptosis detection

Phosphatidylserine (PS) externalization was examined with a two colour analysis of FITC-labeled annexin V binding and PI uptake. The assay was performed by Human Annexin V/FITC kit (Bender MedSystem) according to the manufacturer's instructions. The fluorescence distribution was displayed as dot plot analysis (electronic compensation was required to exclude overlapping of the two emission spectra), and the percentage of fluorescent cells in each quadrant was determined. This test allows for the discrimination of live cells (unstained with either fluorochrome – gated in the lower left quadrant: annexin$^-$/PI$^-$) from early apoptotic cells (stained only with annexin V – gated in the lower right quadrant: annexin$^+$/PI$^-$), late apoptotic cells (stained with both annexin V and PI – gated in the upper right quadrant: annexin$^+$/PI$^+$) or necrotic cells (stained only with PI – gated in the upper left quadrant: annexin$^-$/PI$^+$).

2.4.3. Mitochondrial membrane potential changes

Treated and control cells were loaded with 5 nM tetramethylrhodamine ethyl ester (TMRE), a potential sensitive probe [24]. After 30 min, fluorescence intensity was evaluated by flow cytometry (FL-2 channel).

2.4.4. Intracellular redox state

2′,7′-Dichlorodihydrofluorescein diacetate (DCFH-DA) was used as a probe for intracellular reactive oxygen species (ROS) formation [25]. Briefly, at the end of the incubation time, cells were washed and resuspended (1×10^6 cells/ml) in serum-free medium containing 10 μM DCFH-DA. Following further 30 min of incubation at 37 °C, DCF fluorescence was monitored by flow cytometry (FL-1 channel). In some experiments, cells were double loaded with DCFH-DA and PI to monitor simultaneously the level of ROS–oxidized fluorescent product, DCF, and the integrity of plasma membrane (membrane leakage might cause an increase of DCF efflux).

Free Ca^{2+} concentrations were determined using the calcium indicator dye, Fura-2. Cells, suspended in a HEPES-based Ca^{2+}-free buffer (plus 5 mM dextrose), were incubated with 5 μM fura-2 acetoxymethyl (AM) ester for 60 min at 37 °C to convert the ester to Fura-2. After washing, Fura-2 loaded cells were resuspended in RPMI 1640 (serum- and phenol red-free) at 1×10^4/ml density.

Fluorescence was monitored on a luminescence spectrometer (LS55, PerkinElmer Life Science). Fura-2 was excited at alternating wavelengths of 340 and 380 nm and emission was recorded at 510 nm. Increased 340/380 ratios indicate elevated intracellular $[Ca^{2+}]$. In long-term experiments, cells were exposed to vehicle or SR141716 for the established times before Fura-2 loading. In short term experiments, Fura-2 loaded cells were added to a cuvette and analyzed to establish a baseline before the addition of stimuli. Thapsigargin (200 nM) was used as positive control (340/380 ratio: 1.97 ± 0.12).

2.5. Light and fluorescence microscopy

Cells were stained with crystal violet (0.1% in PBS/20% MeOH) for whole cell morphological analysis. Hoechst 33342 (10 μg/ml) staining was used for apoptotic nuclei determination. Cells were analyzed by the Zeiss Axiovert 200 microscope at Hoechst 33342 fluorescence region (excitation, 351 nm; emission, 380 nm).

2.6. Western blot analysis

Whole lysates for immunoblot analysis were prepared according to standard protocols. Cytosolic protein extracts for determining cytochrome *c* and AIF release were prepared as follows: cells (2×10^6) were gently lysed for 2 min in 80 μl ice-cold lysis buffer (250 mM sucrose, 1 mM EDTA, 20 mM Tris–HCl pH 7.2, 1 mM DTT, 10 mM KCl, 1.5 mM $MgCl_2$, 5 μg/ml pepstatin A, 10 μg/ml leupeptin, 2 μg/ml aprotinin) containing digitonin 0.05%. Protein concentration in samples was determined by Bio-Rad DC Protein Assay. Clarified cell lysates or cytosolic fractions were subject to SDS-PAGE (20–50 μg/lane) under reducing conditions. The percentages of polyacrylamide were 15%, 10% or 8% chosen on the basis of the MW of the protein to detect. Proteins were then transferred onto nitrocellulose membranes and immunoblotted with different primary antibodies. Signals were visualized with appropriate horseradish peroxidase-conjugated secondary antibodies and enhanced chemiluminescence (Amersham, USA).

2.7. Statistical analysis

Unless otherwise specified data reported in each figure are the mean value ± SD of at least three experiments performed in duplicate. Differences between treatment groups were analyzed by the Student's *t* test. Differences were considered significant when $p < 0.05$.

3. Results

3.1. Cell growth inhibition

To determine the effect of SR141716 on cell growth, leukemia-derived Jurkat and U937 cells and non-stimulated freshly isolated PBMC, taken as normal cell counterpart, were exposed to increasing concentrations of SR141716 or vehicle only and the number of viable cells was measured after 24 h. As shown in Fig. 1A, SR141716 inhibited the growth of both leukemia-derived cell lines in a dose- and time-dependent manner. Dose–response curves were obtained in a narrow range of doses. SR141716 exhibited low or no cell growth inhibition activity at concentrations lower than 5 μM, but was highly cytotoxic at 20–25 μM. The SR141716 inhibitory effect was more pronounced, especially at the lowest doses, in Jurkat than in U937 cells. The half maximal

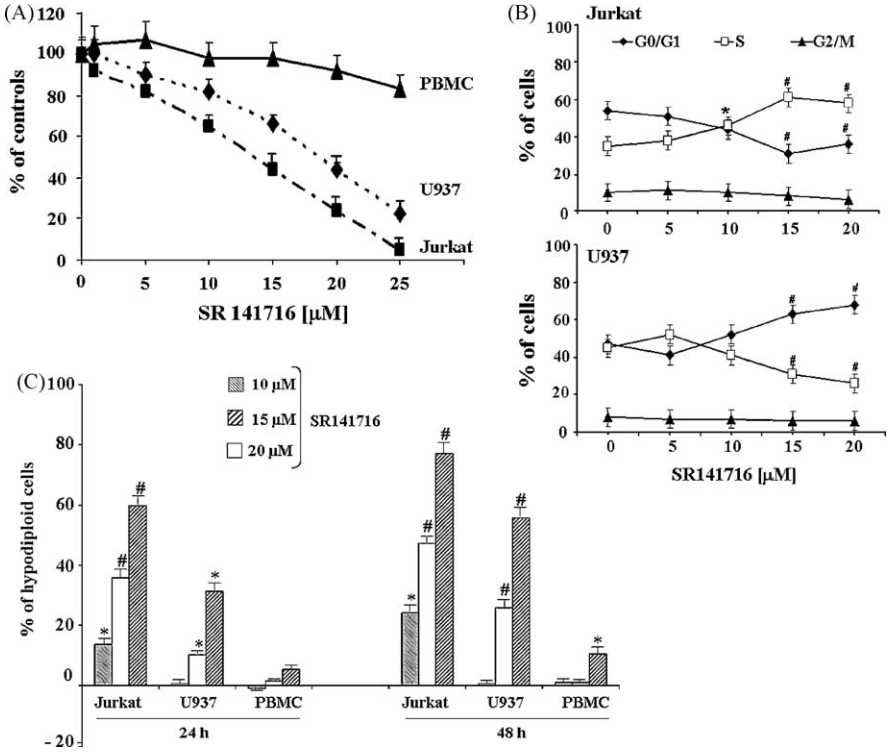

Fig. 1. SR141716 cytotoxic and cytostatic effects. Jurkat and U937 cells and non-stimulated freshly isolated PBMC were exposed to increasing doses of SR141716 or vehicle only as controls. (A) The number of viable cells was evaluated after 24 h treatment; data are expressed as percentages of the respective controls; the number of control leukemia cells after 24 h incubation was more than doubled; the number of control non-proliferating PBMC after 24 h incubation was slight lower (about 10%) than at time 0. (B) The distribution of Jurkat, U937 cells and the respective controls in the different phases of cell cycle was measured 24 h following treatment. (C) Percentages of hypodiploid cells in SR141716-treated Jurkat, U937, and PBMC cells after subtracting the respective control values (24 h incubation: $2.3 \pm 0.05\%$, $2.7 \pm 0.45\%$, and $10.11 \pm 0.1\%$, in Jurkat, U937, and PBMC, respectively; 48 h incubation: $3.8 \pm 0.07\%$, $4.2 \pm 0.04\%$, and $19.8 \pm 2.05\%$ in Jurkat, U937, and PBMC, respectively). All data are shown as means ± SD of at least three experiments each done in triplicate ($^*p < 0.05$ and $^\#p < 0.01$ vs. control).

inhibitory concentration (IC50) values were 13 μM and 18 μM in Jurkat and U937, respectively. In contrast, SR141716 slight affected PBMC viability, as the number of trypan blue positive cells increased only at the highest doses tested.

The effect of SR141716 on Jurkat and U937 cell viability was evaluated also at 48 h treatment. The half maximal inhibitory concentration (IC50) values, calculated on the basis of dose–response curves at 48 h (data not shown), were 6 and 10 μM in Jurkat and U937, respectively (about one half those calculated at 24 h).

3.2. Cell cycle analysis and sub-G1 DNA measurement

Since the decrease in the cell number may result from cell cycle arrest and/or cell death, we first examined whether SR141716 affected Jurkat and U937 cell cycle progression. As shown in Fig. 1B, 24 h SR141716 treatments caused different effects on Jurkat and U937 cell cycle progression. In Jurkat cells, the drug induced a dose-dependent increase (at concentrations up to 15 μM) of the percentages of cells in S phase. Conversely, U937 cells accumulated dose-dependently in G_0/G_1 at all SR141716-tested doses, except at the lowest (5 μM), where a delay in S-phase transition was detectable. Substantially similar results were observed at 48 h (data not shown).

In addition to cytostatic potential, SR141716 also exhibited cytotoxic activity in both Jurkat and U937 cells (Fig. 1C). After 24 h incubation, we observed a dose-dependent increase of Jurkat and U937 cells in sub-G_0/G_1. Jurkat cells proved more susceptible to SR141716 cell death-promoting activity than U937. Conversely, non-stimulated PBMC resulted quite resistant to SR141716 cytotoxic effect, since a slight increase of the percentages of hypodiploid cells was detectable only at the highest SR141716 dose tested (20 μM). After 48 h incubation, a further increase of the percentages of hypodiploid cells was observed in Jurkat cells at all tested SR141716 doses; in U937 and non-stimulated PBMC, a time-dependent increase of hypodiploidia was detectable at doses ≥15 μM and >20 μM, respectively. However, it should be underlined that the percentages of dying cells in control PBMC maintained in culture for 48 h in the absence of mitogenic stimuli was quite high (~30%, and ~20% underwent apoptotic death), thus the possibility that the forced conditions make these primary cells more susceptible to exogenous toxic stimuli cannot be excluded.

3.3. Characterization of SR141716 cell death-promoting activity

The observed increase of cells with a DNA content lower than G_1 (hypodiploidia) suggested that SR141716 promoted cell death by, at least partly, activating apoptotic processes. To better discriminate between apoptosis and necrosis (sub-G_1 cell count might also include necrotic cells), we performed the annexin V-FITC/PI test. Jurkat and U937 cells were treated with SR141716 at doses close to the respective IC50 values (15 μM and 20 μM, respectively). These doses were used to obtain comparable levels of cell death in the two cell lines and, unless otherwise specified, were used in all the subsequent experiments. Representative cytograms in Fig. 2A(a) (cytograms on the top), show that 24 h exposure to SR141716 caused an increase of the percentages of cells gated in the upper right quadrant (annexin$^+$/PI$^+$, late apoptotic/necrotic cells) and, to a lower extent, of cells in the lower right quadrant (annexin$^+$/PI$^-$, early apoptosis). In particular, after subtracting the respective control values, the ratio between annexin$^+$/PI$^-$ and annexin$^+$/PI$^+$ cell populations was about 0.5 in Jurkat and only 0.1 in U937 cells. Since the majority of dying cells were positive for annexin V labeling, but also

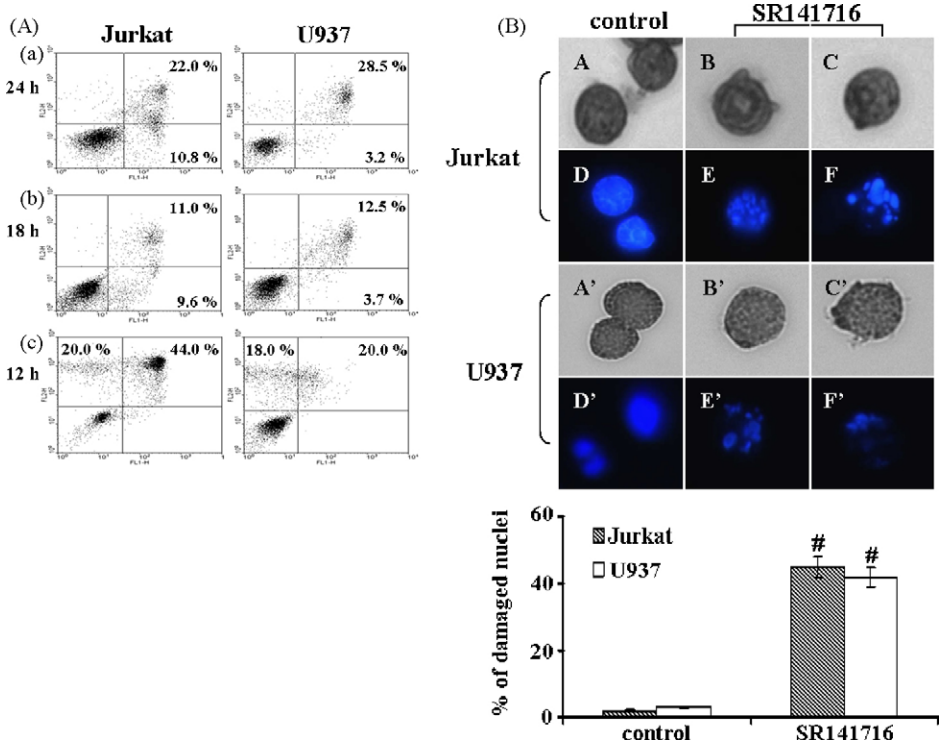

Fig. 2. SR141716-induced phosphatidyl serine exposure and chromatin condensation. (A) Control and cells exposed to SR141716 were double stained with annexin V-FITC and PI under non-permeabilized conditions and analyzed by flow cytometry. Jurkat and U937 cells were exposed for the indicated times to 15 μM and 20 μM (a, b) or 25 μM and 30 μM (c) SR141716, respectively. The analysis regions were set such that ≤2% of control cells were positive for annexin V-FITC/PI. Cytograms are representative of at least three experiments with similar results. (B) Cell and nuclear morphology. Light (crystal violet staining) and fluorescence (Hoechst 33342 staining) microscopy (400× magnification) analysis of Jurkat and U937 exposed to vehicle alone (A, D and A′, D′) or to 15 μM (B, E and B′, E′) and 20 μM (C, F and C′, F′) SR141716, respectively, for 24 h. Lower panel: percentage of apoptotic cells based on counting approximately 100 cells. Error bars indicate ± SD of thee independent experiments ($^{\#}p < 0.01$ vs. control).

permeable to PI, we wondered whether these cells derived from apoptotic cells that acquired membrane incompetence (secondary necrotic death) or were an artifact due to staining of intracellular phosphatidylserine (PS) in membrane-compromised primary necrotic cells. Firstly, in the attempt to delay the kinetics of cell transition from the lower left to the upper left quadrant, we examined the annexin V/PI profiles of cells exposed to SR141716 for a time shorter than 24 h. Representative cytograms in Fig. 2A(b) (cytograms in the middle) illustrated that, after 18 h treatment, the annexin$^+$/PI$^-$ to annexin$^+$/PI$^+$ ratio increased up to ~0.9 in Jurkat, but less than ~0.3 in U937 cells. Next, Jurkat and U937 were exposed 12 h to 25 μM and 30 μM SR141716, respectively, two highly cytotoxic concentrations. As indicated by cytograms on the bottom of Fig. 2A, a typical necrotic profile (being the most of the cells positive for PI uptake, but negative for annexin V staining) was obtained. Taken together, the above results suggest the occurrence of mainly secondary necrosis, especially in Jurkat cells, and exclude artificial intracellular PS staining due to PI influx.

To gain more insight into the SR141716-induced apoptotic mode of cell death, we examined cell and nuclear morphology in treated and control leukemia cells by light and fluorescence microscopy. After 24 h of treatment, SR141716 caused morphological changes characteristic of apoptosis such as features of membrane blebbing and nuclear disintegration in both Jurkat and U937 cells (Fig. 2B). Hoechst 33342 staining demonstrated a significant increase of DNA fragmentation in treated cells compared to controls.

3.4. SR141716 induces loss of mitochondrial membrane potential and Ca^{2+} elevation

Since mitochondria play a critical role in the regulation of both apoptotic and necrotic cell death [26], we evaluated the effect of SR141716 on mitochondrial membrane potential ($\Delta\Psi$m). Jurkat and U937 cells were exposed to increasing doses of SR141716 and analyzed after 24 h for both the loss of $\Delta\Psi$m and the extent of PS exposure on plasma membrane (annexin$^+$/PI$^-$ plus annexin$^+$/PI$^+$ cell populations). Curves reported in Fig. 3A show that SR141716 induced a robust $\Delta\Psi$m loss in both cell lines. Interestingly, the percentage of cells with depolarized mitochondria was higher, especially in U937, than that of annexin$^+$ cells measured at the same drug concentrations. Data summarized in Fig. 3B indicate that SR141716-induced $\Delta\Psi$m loss occurred earlier than PS exposure especially in U937 cells, where mitochondria depolarization was detectable also in the absence of any apoptotic death sign.

Because Ca^{2+} elevation has been shown to contribute to mitochondrial dysfunction [27], the effect of the cell permeable Ca^{2+} chelator BAPTA-AM on SR141716-induced mitochondria depolarization was evaluated. By preventing Ca^{2+} elevation, the extent of SR141716-induced mitochondria depolarization was significantly attenuated in U937 cells (cytograms in Fig. 3C), but not in Jurkat cells (data not shown). This result prompted us to evaluate the effect of SR141716 on intracellular Ca^{2+} elevation. When U937 cells were incubated with the drug for 1, 3, 6 and 12 h before Fura-2 loading, we did not measure any increase of the 340/

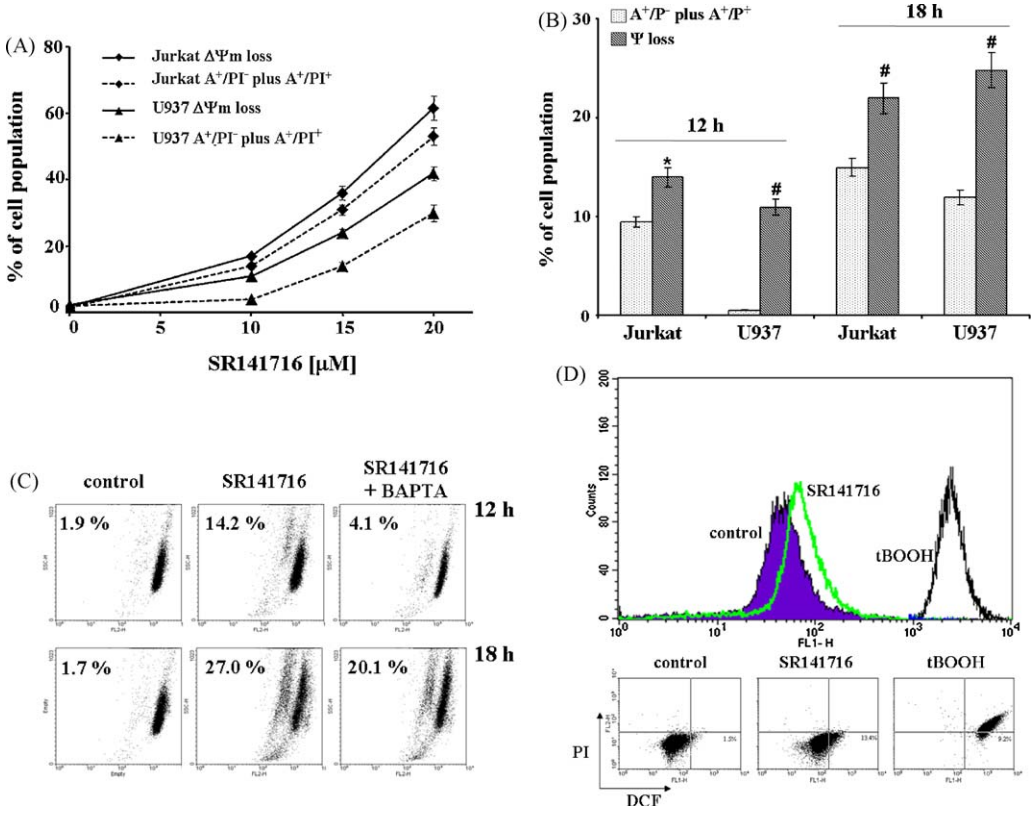

Fig. 3. SR141716-induced mitochondrial depolarization and changes in Ca^{2+} and ROS levels. (A) Mitochondrial membrane depolarization ($\Delta\Psi$m loss) and PS exposure (annexin V-FITC positive cells, A$^+$/PI$^-$ plus A$^+$/PI$^+$) in Jurkat and U937 cells exposed to increasing doses of SR141716 or vehicle for 24 h. Data are shown as means ± SD of at least three experiments performed in duplicate. (B) Mitochondrial membrane depolarization and PS exposure in Jurkat and U937 cells exposed to 15 μM and 20 μM SR141716, respectively, for the indicated times. Data, subtracted for control values, are shown as means ± SD of two experiments performed in duplicate ($^*p < 0.05$ and $^\#p < 0.01$ $\Delta\Psi$m loss vs. PS exposure). (C) Protective effect of Ca^{2+} chelation on the extent of $\Delta\Psi$m in U937 treated with 20 μM SR141716 for the indicated times. Cytograms are from one experiment of three with similar results. (D) ROS levels in U937 exposed to vehicle only (control), 300 μM t-BOOH (positive control) and 20 μM SR141716 for 3 h; cells were loaded with DCFH-DA alone (upper panel) or with both DCFH-DA and PI (lower panel). The figures are representative of three independent experiments.

380 ratio. However, by lowering the exposure time to 10 min, the 340/380 ratio in 20 μM SR141716-treated cells increased from 1.06 ± 0.09, the value recorded in control cells, to 1.37 ± 0.13, thus suggesting that the drug triggered a rapid intracellular Ca^{2+} elevation. Our results on the role of Ca^{2+} in SR141716-induced U937 cell death are also supported by previous studies showing that U937 cells possess a Ca^{2+}-dependent apoptosis pathway [28,29].

Mitochondrial damage and subsequent cell death are often dependent upon drug-induced oxidative stress. Thus, we evaluated SR141716 pro-oxidant potential by measuring DCFH-DA ROS-mediated oxidation in Jurkat and U937 cells. Cells were exposed to the drug for times ≤3 h, because at longer times ROS elevation might be a consequence, rather than a cause, of mitochondrial dysfunctions. While SR141716 did not cause any increase of ROS production in Jurkat cells (data not shown), it induced a slight dose-dependent elevation of ROS in U937 cells. In particular, at 30, 90 and 180 min, the percentage of DCF green fluorescence positive cells increased by 3%, 5% and 13%, respectively (representative histograms obtained after 3 h incubation are reported in Fig. 3D, upper panel). The absence of PI red fluorescence positive cells allowed us to exclude that the slight ROS elevation observed was due to increased DCF efflux occurring in membrane-compromised cells (Fig. 3D, lower panel).

3.5. Cytochrome c and AIF release

The cytosolic release of mitochondrial pro-apoptotic proteins is one of the key events in the mitochondria-dependent apoptotic death process [30]. In particular, cytochrome *c* and apoptosis-inducing factor (AIF) are two important effectors of caspase-dependent and caspase-independent cell death programs.

Blots in Fig. 4A show that cytochrome *c* (panel A) was present in the mitochondria-free cytosolic fractions from both Jurkat and U937 cells exposed 12 h to SR141716, but not in the corresponding controls. SR141716 treatment induced also mitochondrial AIF release, even though the process turned out to occur later than cytochrome *c* release (Fig. 4B); in fact immunoreactive AIF signals were detectable 18 h, but not 12 h (data not shown) after treatment. Moreover, while the amount of cytosolic cytochrome *c* was almost comparable in the two leukemia cell lines, the levels of released AIF was higher in U937 than in Jurkat cells. Interestingly, the AIF immunoreactive signal in both the cytosolic fractions and whole lysates of SR141716-exposed cells appeared as a doublet rather than a single band, suggesting a protease-mediated cleavage of AIF from its native form (MW 67 kDa) to the N-terminal-truncated forms (57–62 kDa) [31].

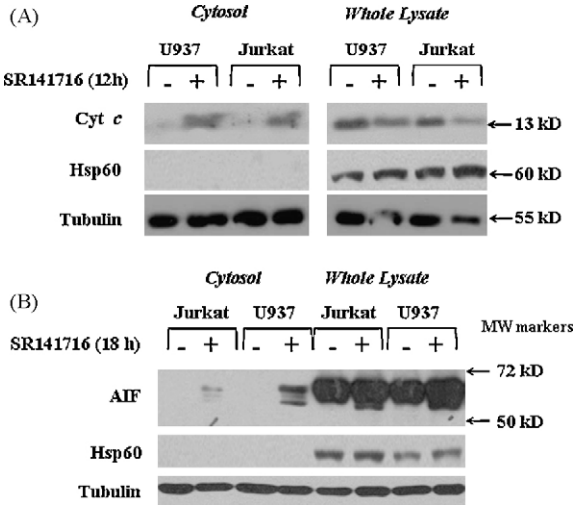

Fig. 4. SR141716-induced release of cytochrome *c* and AIF. Jurkat and U937 cells were exposed for the indicated times to 15 μM and 20 μM SR141716, respectively, or to vehicle only. Cytosolic fractions and whole lysates were probed with anti-cytochrome *c* (A) and anti-AIF (B) antibodies. Blots were reprobed with anti-Hsp60 and, subsequently, with anti-tubulin antibodies to check the purity of the cytosolic fractions and protein loading, respectively. Results from a single experiment out of three experiments with similar results are showed.

3.6. Role of caspases in SR141716-induced cell death

We evaluated the contribution of caspase pathways to SR141716-induced apoptosis and mitochondrial dysfunction by means of ZVAD, a pan-caspase inhibitor. SR141716-treated Jurkat and U937 cells were incubated 24 h in the absence and in the presence of ZVAD and after the incubation, the percentage of annexin$^+$ cells and cells with reduced mitochondrial potential were evaluated (Fig. 5A). In Jurkat cells, the caspase inhibitor reduced the levels of PS exposure by ∼60%; the effect was particularly marked on the percentages of annexin$^+$/PI$^-$ (early apoptotic cells), which dropped to control values (representative cytograms in the insert). In U937 cells, the contribution of the caspase pathways to SR141716-induced cell death seemed to be lower than in Jurkat cells, as ZVAD reduced the percentage of annexin$^+$ cells by less than 35%. Caspase inhibition likely had a lower protective effect against $\Delta\Psi$m loss than PS exposure, as mitochondrial potential dissipation was reduced by ∼45% in Jurkat and less than ∼20% in U937 cells. This result suggested that caspase pathway activation by SR141716 occurred mainly downstream of mitochondria.

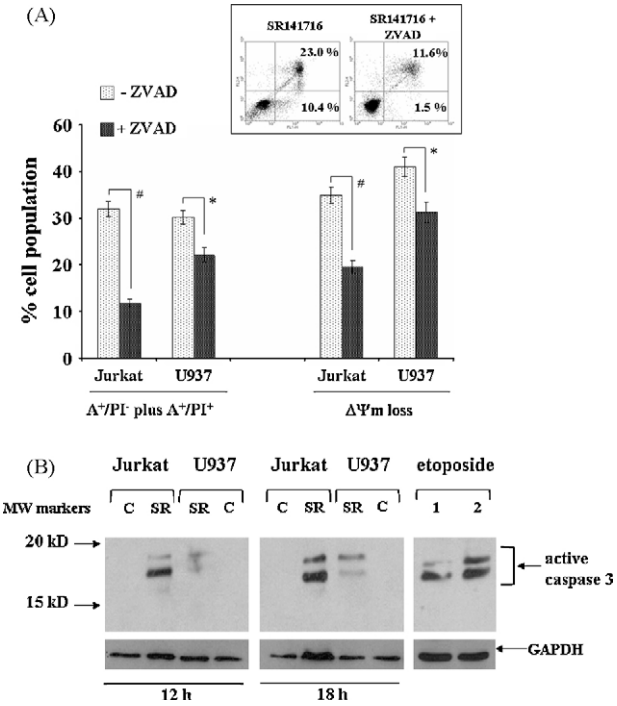

Fig. 5. Role of caspases in SR141716-induced cell death. (A) Effect of ZVAD (20 μM) on SR141716-induced PS externalization (annexin V-FITC positive cells, A$^+$/PI$^-$ plus A$^+$/PI$^+$) and $\Delta\Psi$m loss in Jurkat and U937 cells exposed 24 h to 15 μM and 20 μM of the drug, respectively. Reported results are the means ± SD of at least three experiments performed in duplicate ($^*p < 0.05$ and $^\#p < 0.01$ vs. samples without ZVAD). Representative cytograms of SR141716-treated Jurkat cells in the absence and in the presence of ZVAD are shown in the insert (the analysis regions were set such that <2% of the control cells were positive for annexin V-FITC/PI). (B) Caspase 3 activation. Whole lysates from Jurkat and U937 cells, exposed for the indicated times to SR141716 (SR) 15 μM and 20 μM, respectively, were checked for caspase 3 proteolytic cleavage. Cells treated with the vehicle alone (C) were used as negative control. Jurkat cells (lane 1) and U937 cells (lane 2) treated with 10 μM etoposide for 24 h were used as positive controls. GAPDH was used for normalization. MW markers are indicated on the left. Blots from a single experiment representative of at least two with similar results are reported.

Since ZVAD has been shown to inhibit other proteases [32], we needed to establish unequivocally the presence of a caspase-dependent component in the SR141716-induced cell death program. Because of the key role of mitochondria in SR141716-induced cell death, we focused on caspase 3 as this effector caspase is generally activated succeeding mitochondrial depolarization and release of cytochrome *c*. SR141716 treatment caused caspase 3 cleavages in both Jurkat and U937 cells, as two bands with an apparent MW of 19 and 17 kDa were detectable (Fig. 5B). However, in U937, caspase activation was likely to occur later and to a lower extent than in Jurkat cells.

3.7. Role of PARP1 in SR141716-induced leukemia cell death

Poly(ADP-ribose) polymerase (PARP1), apart from its role as a DNA repairing enzyme, is an important activator of caspase-independent cell death via promoting AIF release [33]. Thus, we investigated whether PARP1 activation played some role in the non ZVAD-inhibitable component of the SR141716 cell death program. We evaluated the effect of PJ34, a PARP1 inhibitor, on the extent of SR141716-induced PS exposure (annexin$^+$/PI$^-$ plus annexin$^+$/PI$^+$cells) and mitochondrial depolarization. In Jurkat cells we found that PJ34 has only a marginal or no protective effect against the increase of annexin$^+$ cells and $\Delta\Psi$m loss. Furthermore, the effects of combined PJ34 and ZVAD were comparable to ZVAD alone. Conversely, in U937 cells, pharmacological inhibition of PARP1 activity reduced the percentage of cells with altered $\Delta\Psi$m by 50% and that of cells positive for annexin labeling by ~33% (Fig. 6A). Interestingly, the annexin$^+$/PI$^-$/annexin$^+$/PI$^+$ ratio increased from 0.08 to 1.8 (Fig. 6B), thus indicating that PJ34 prevented, at least in part, the rapid shift of cells from the early apoptotic to the late apoptotic/necrotic phenotype. The protective effect of PJ34 and ZVAD co-administration turned out to be additive in agreement with the hypothesis that both caspase-dependent and caspase-independent (PARP1-mediated) pathways contributed to the SR141716-induced cell death execution program.

To confirm the role of PARP1-pathway in SR141716-induced U937 cell death, we evaluated the activation of this enzyme by measuring the level of protein poly(ADP-ribosyl)ation (PAR) by WB. Extensive protein PARylation, almost completely prevented by PJ34, was observed in U937 cells (Fig. 6C). PAR formation was detectable as early as 4 h after SR141716-exposure, thus indicating that PARP1 activation occurred before $\Delta\Psi$m loss and PS exposure (see Fig. 3). Interestingly, the intensity of PAR protein signal, after a maximum at 8 h, began to decrease at 12 h.

Such a decrease suggested the onset of processes counteracting sustained PARP1 activation and the subsequent PARP1-dependent necrotic cell death [34]. As PARP1 cleavage by caspase 3 to a non-functional 89 kDa peptide is known to be crucial for the shift from the necrotic to the apoptotic program, we evaluated the presence of this proteolytic fragment in SR141716-treated Jurkat and U937 cells. Blots reported in Fig. 7(A and B) show that SR141716 caused a dose- and time-dependent increase of the signals at 89 kDa concomitant with a decrease of the full-length protein band in both cell lines. Surprisingly, PARP1 cleavage turned out to be more extensive (there was a higher ratio between the cleaved/native forms of PARP1) and to occur earlier in U937 than in Jurkat cells. In another set of experiments we verify whether PARP1 digestion was inhibited by ZVAD. Fig. 7C shows that while PARP1 digestion was completely inhibited by ZVAD in Jurkat cells, the 89 kDa fragment intensity was only attenuated by the caspase inhibitor in U937 cells. This result suggested that, in U937 cells, other proteases might contribute to the higher extent of PARP1 processing. For instance, PARP1 is also a substrate for cathepsins and calpains [35,36]. However, in SR141716-treated U937 cells we did not observe any of the PARP1 fragments known to be produced by these lysosomal proteases (see Fig. 7C). Moreover, both the calpain

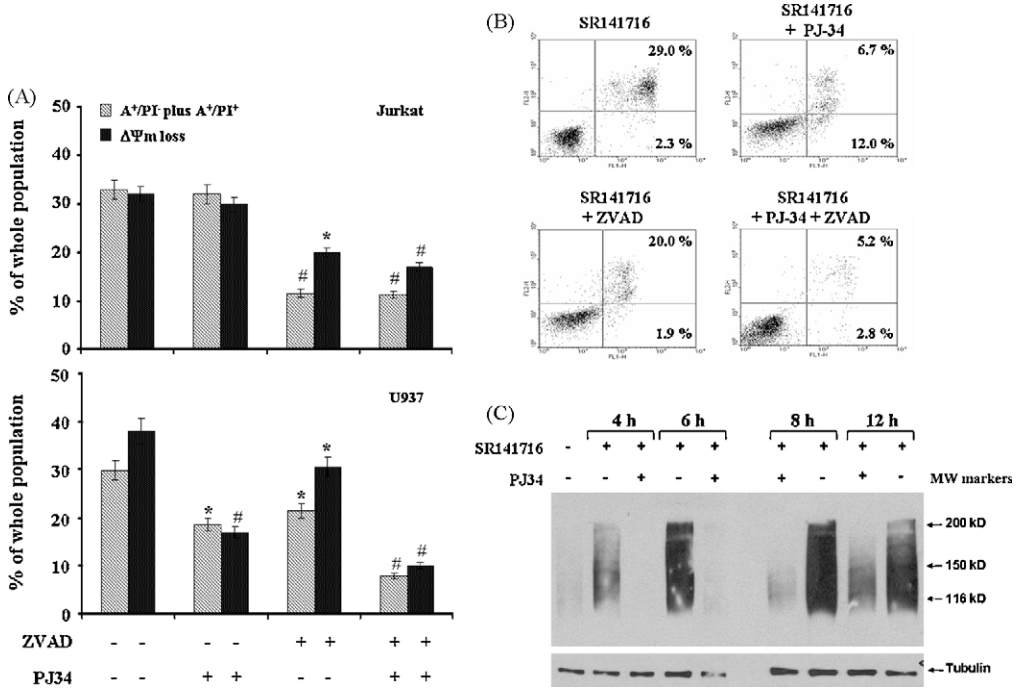

Fig. 6. Role of PARP1 activation in SR141716-induced cell death. (A) Effect of PJ34 (4 μM), alone or given in combination with ZVAD (20 μM), on SR141716-induced increase of PS externalization (annexin V-FITC positive cells, A$^+$/PI$^-$ plus A$^+$/PI$^+$) and $\Delta\Psi$m loss. Jurkat and U937 cells were exposed 24 h to 15 μM and 20 μM SR141716, respectively. Data are shown as means ± SD of at least three experiments each done in duplicate ($^*p < 0.05$ and $^\#p < 0.01$ vs. cells treated with SR141716 alone). (B) Representative cytograms of annexin V-FITC/PI doubled stained U937 cells exposed 24 h to 20 μM SR141716 in the absence or in the presence of the inhibitors as indicated in the figure. The analysis regions were set such that <2% of the control cells were positive for annexin V-FITC/PI. Cells exposed to ZVAD or PJ34 alone gave profiles comparable to that of control cells (not shown). (C) Whole cell lysates from U937 exposed for the indicated times to 20 μM SR141716 were probed with PAR antibody. Lanes 1, cells treated 8 h with vehicle only. Tubulin was used for normalization. Blots from a single experiment representative of two with similar results are reported.

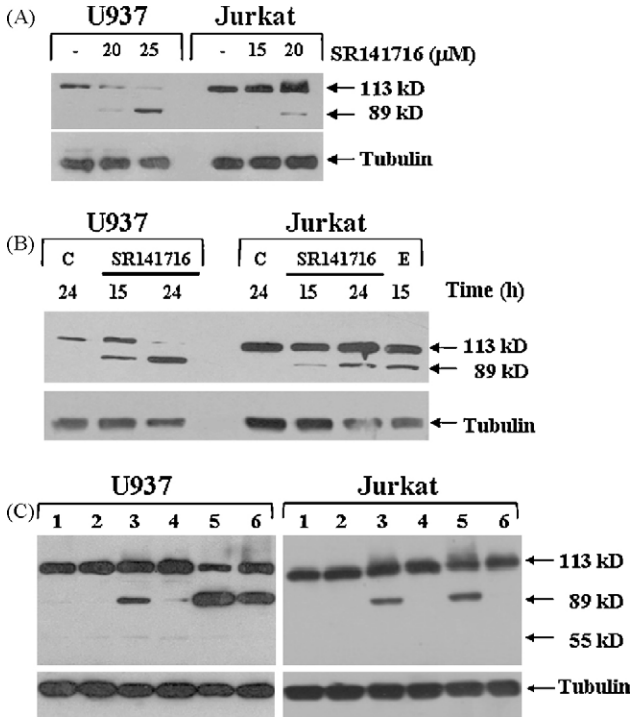

Fig. 7. PARP1 processing in SR141716-treated Jurkat and U937 cells. PARP1 processing was evaluated in whole lysates from Jurkat and U937 cells exposed 24 h to different doses of SR141716 (A) or to 15 μM and 20 μM of the drug, respectively, for the indicated times (B). Cells exposed to vehicle only (C) or etoposide (E) were used as negative and positive controls, respectively. (C) Effect of ZVAD on PARP1 cleavage in Jurkat and U937cells exposed 24 h to 15 μM and 20 μM SR1411716, respectively. Treatment were shown as: vehicle (lane 1), ZVAD (lane 2), etoposide (lane 3), etoposide + ZVAD (lane 4), SR141716 (lane 5), SR141716 + ZVAD (lane 6). Tubulin was used for normalization. Blots from a single experiment representative of at least two with similar results are reported.

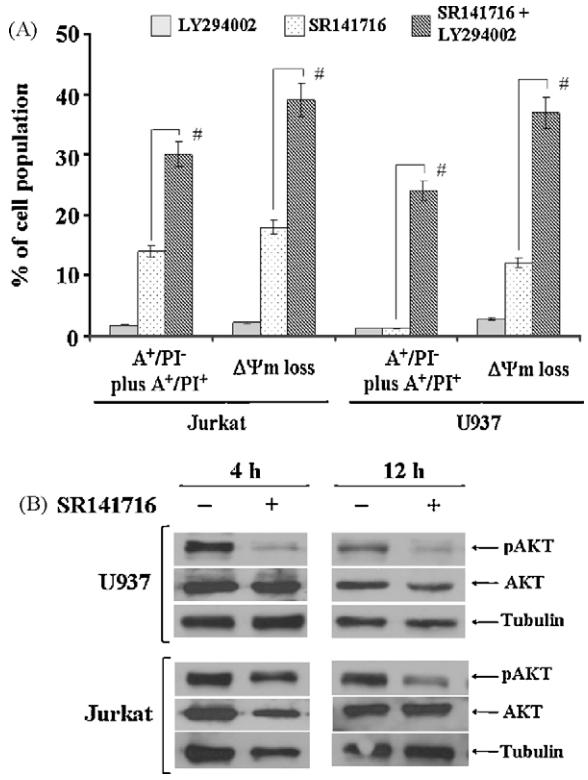

Fig. 8. Involvement of PI3K/AKT pathway in SR141716-induced effects. (A) Jurkat and U937 cells were exposed 12 h to LY294002 alone or in combination with 15 μM and 20 μM SR141716, respectively. Cells exposed to vehicle were included as controls. The percentages of annexin V-FITC positive cells (A^+/PI^- plus A^+/PI^+) and of those with reduced $\Delta\Psi m$ were evaluated by flow cytometry. Data are the means ± SD of three independent experiments performed in duplicate ($^*p < 0.05$ and $^\#p < 0.01$ vs. in the absence of LY294002). (B) Whole cell lysates from Jurkat and U937 exposed for the indicated times to 15 μM and 20 μM, respectively, were checked for the level of AKT and its phosphorylated form (pAKT). Tubulin was used for normalization. The figure is one representative of three with similar results.

inhibitor I and Z-FA-fmk, a broad spectrum inhibitor of cathepsins, failed to reduce the intensity of the 89 kDa signal (data not shown).

3.8. PI3K/AKT pathway has a survival role in SR141716-induced cell death

Since the PI3K/AKT pathways are well-characterized cell survival signalling pathways that block apoptosis in a variety of cell types [37–39], we examined the role of PI3K-dependent signals in counteracting SR141716-induced cell death by means of a pharmacological approach. In preliminary experiments we found that the combined treatment with SR141716 and LY294002, a selective P13K inhibitor, caused extensive cell death at 24 h. Thus, in subsequent experiments the effect of PI3K inhibition was quantified as early as 12 h after treatment (Fig. 8A). Especially in U937, the presence of LY294002 strongly increased the extent of SR141716-induced mitochondria depolarization and PS exposure. Next we evaluated whether SR141716 by itself had some effect on the activation of PI3K/AKT pathways. Blots reported in Fig. 8B show that SR141716 decreased the extent of constitutive AKT phosphorylation in both cell lines, without affecting the protein level. Interestingly, in U937, the reduction of pAKT signal was more marked and earlier detectable than in Jurkat cells.

4. Discussion

In this study we investigated the in vitro effects of SR141716, a CB1 antagonist, on cell growth, morphology, cell cycle and death in Jurkat and U937, two leukemia-derived cell lines, and examined the mechanisms underlying its actions. We found that SR141716 is an effective tumor cell growth inhibitor, displaying IC50 values of 13 and 18 μM in Jurkat and U937 cells, respectively, at 24 h incubation and still lower values at 48 h. On the other hand, SR141716 doses up to 25 μM slightly reduced the number of non-stimulated freshly isolated PBMC, taken as normal cell counterpart.

SR141716 reduced the number of proliferating cells by activating, to a different extent, both cell cycle arrest and cell death responses. In Jurkat cells, SR141716 primarily exhibited a cell death-promoting activity, while in U937 cells it elicited mainly cytostatic effects. Indeed, the G_0/G_1 arrest of U937 cells might likely be a condition responsible of the higher resistance of this cell line to the onset of cell death program. The hypothesis that G_0/G_1 cell cycle arrest might have some protective role against SR141716-induced death might be partially supported by results previously obtained on proliferating PBMC [19]. The work showed that SR141716 significantly inhibited the proliferative response of stimulated PBMC by inducing a G_0/G_1 block, without inducing apoptosis and cell death. However, if the quiescent status (G_0/G_1 block) was likely to make PBMC quite resistant to SR141716-triggered death stimuli, the same G_0/G_1 block induced in U937 by SR141716 delayed, but did not prevent subsequent cell death. A possible explanation of the different capabilities of U937 cells and PBMC to counteract SR141716 cell death-promoting activity might lie in the different effects of the drug on PI3K/AKT pathways, known to contribute to apoptosis-resistance [37–39]. In PBMC, SR141716 was found to increase the levels of pAKT [19], while here we showed that in U937 cells the drug decreased, as early as 4 h following treatment, the level of pAKT as compared to untreated

controls. Previous studies in p53-defective hematopoietic tumor cells have shown that the p53-independent G1 arrest in response to toxic agents can be overridden by the PI3K/AKT pathway [40]. Thus, the observed early down-regulation of this pathway might allow U937, lacking p53, to accumulate in G_0/G_1 as a primary defensive condition. Yet, just the inactivation of PI3K/AKT pathways – which normally is sustained in leukemia-derived cells – was likely to make U937 more responsive than their normal counterparts to further SR141716-triggered death stimuli. PI3K pharmacological inhibition by LY294002 increased SR141716 death response, thus indicating that SR141716 reduced, but did not abrogate, PI3K/AKT signals and confirmed the key role of this pathway in leukemia-derived cell survival [38–41].

It has been reported that several natural and synthetic cannabinoids activate cell death-promoting signals through mechanisms independent of CB receptor engagement [15,16,42]. Similarly, the SR141716 cytotoxic effects against leukemia cells was not likely to be dependent on SR141716-CB1 complex triggered signals. This was suggested by the following observations: (i) cytotoxic effects were detectable only at concentrations that far exceed those ($\leq$5 μM) used in CB1 competition experiments [15]; and (ii) in agreement with previous studies [15,42], we found that the expression of CB1 was very low (Jurkat) or absent (U937) in leukemia-derived cells used in the present study (data not shown).

Concerning the mechanisms of SR141716-induced cell death, we found that Jurkat and U937 treated cells displayed hypodiploidia, PS exposure and dissipation of mitochondrial membrane potential, typical, even if not exclusive, markers of the apoptotic mode of cell death. However, after 24 h incubation with SR141716, most of the PS-exposing cells, especially in U937 cells, were also positive for PI uptake, indicative of necrosis- or late apoptosis-associated plasma membrane leakage. By shortening SR141716 treatments to times lower than 24 h, the transition kinetics from the annexin$^+$/PI$^-$ to annexin$^+$/PI$^+$ phenotype was delayed in Jurkat, thus supporting that in this cell line the annexin$^+$/PI$^+$ population mostly included late apoptotic cells, rather than primary necrotic cells. Conversely, in U937 PS exposure was associated with plasma membrane permeabilization at 24 h and shorter incubation times. This may suggest that SR141716 activated necrotic death in U937. However, SR141716 caused extensive chromatin condensation and fragmentation not only in Jurkat, but also in U937. Thus, on the basis of nuclear morphology postulating that necrotic cell death occurs without nuclear condensation [43] and further evidences discussed below, it is conceivable that SR141716 signals could activate in U937 other types of programmed cell death (PCD) processes, rather than simple primary necrosis [44].

Previous studies have shown that TRPV1 (vanilloid) receptor agonists and antagonists (some of which have activity at CB1 and/or CB2 receptors) modulate mitochondrial function, resulting in apoptotic cell death [45] and also demonstrated that natural and synthetic cannabinoids are strong inhibitors of mitochondria functions [46]. Also SR141716-activated signals seemed to converge and integrate at the level of the mitochondria. In fact, consistent with mitochondria-mediated death process, SR141716 caused extensive loss of membrane potential ($\Delta\Psi$m) and release of aptogenic proteins, such as cytochrome *c* and AIF. Mitochondria-dependent death signalling was particularly relevant in U937 cells where depolarization occurred before the appearance of other signs of apoptosis or necrosis. Although some increase in ROS production and Ca^{2+} elevation contributed to $\Delta\Psi$m loss in U937 cells, the mechanisms responsible for SR141716-induced mitochondria dysfunctions remain to be clarified.

Cytochrome *c* is a key mediator of caspase-dependent cell death. After cytochrome *c* is released from the mitochondria, it promotes apoptosome-complex formation and thus caspase pathway activation [reviewed in 30]. Cytochrome *c* release as well as proteolytic cleavage of the death protease caspase 3 was detected in SR141716-exposed Jurkat and U937 cells. The activation of a caspase-dependent pathway by SR141716 in U937 cells was quite surprising, as the fast appearance of cells positive for both annexin V and PI is rather associated with caspase-independent death or necrotic processes [47]. However, the contribution of a caspase-dependent component in SR141716-induced cell death was effectively lower in U937 compared to Jurkat cells. In fact, ZVAD inhibited SR141716-induced cell death by only 35% in U937 and by about 60% in Jurkat cells. The abrogation of caspase pathways by ZVAD was still less effective in preventing, especially in U937 cell line, SR141716-induced mitochondrial potential collapse. In particular, the changes in $\Delta\Psi$m were consistently independent of the caspase inhibitor at short exposure times, confirming that SR141716-induced activation of caspases occurred downstream of mitochondria and possibly that their activation might provide a positive feedback loop, which further compromises mitochondrial integrity.

Along with a minor contribution of ZVAD-inhibitable death pathways [44], SR141716 caused a more pronounced mitochondrial release of the AIF flavoprotein in U937 than in Jurkat cells. Once released from mitochondria, AIF translocates into the nucleus, where it causes chromatin condensation and triggers other signals resulting in PS exposure, large scale DNA fragmentation, and ultimately caspase-independent cell death [47].

PARP1, aside from its main function as a DNA repair enzyme, plays a role in necrotic as well caspase-independent cell death by promoting AIF release [48]. Although the exact mechanisms underlying AIF release from mitochondria are not completely elucidated [49], in the PARP1/AIF-mediated PCD model, the binding of the PAR polymer to acceptor proteins (PAR polymer binding proteins) at the mitochondria is likely to play a role in AIF translocation from the mitochondria to the nucleus [50]. By means of pharmacological approaches and direct measurements of protein PARylation levels we demonstrated the contribution of PARP1 activation in the non ZVAD-inhibitable component of the SR141716-triggered cell death program in U937 cells, but not in Jurkat cells. The PARP1 inhibitor, PJ34, reduced the percentage of U937 PS-exposing cells (annexin$^+$/PI$^-$ plus annexin$^+$/PI$^+$) by about 35%, a value similar to that obtained with ZVAD in this cell line. However, differently from ZVAD, PJ34 was effective in delaying the transition of PS-exposing cells with intact plasma membrane (annexin$^+$/PI$^-$) towards membrane incompetence (annexin$^+$/PI$^+$ cells). Furthermore, we found that: (i) the preventive effect of PJ34 against SR141716-induced mitochondrial depolarization was much more pronounced than that of ZVAD; and (ii) the combined exposure to PJ34 and ZVAD caused additive protective effects on both PS exposure and $\Delta\Psi$m loss. Taken together, our findings suggest that in U937cells, PARP1 activation occurs upstream of the onset of mitochondrial dysfunction and subsequent cell death signals, such as the release of cytochrome *c* and AIF. These proteins mediated, in turn, the caspase-dependent and caspase-independent component of the SR141716-induced cell death program. However, in U937, caspase 3 and other undefined proteases seem to promote a negative feedback loop for the PARP1-triggered non ZVAD-inhibitable pathway. In fact, we observed that extensive PARP1 cleavage to its 89 kDa inactive fragment, a specific product of caspase 3-mediated PARP1 processing, occurred in U937 cells to a greater extent than in Jurkat cells.

In conclusion, SR141716 induces cell cycle arrest and programmed cell death in leukemia-derived Jurkat and U937 cell lines, and, depending on the cell type, activates different as well equivalent death pathways to a different extent. Furthermore, independent of the activated cell death program, SR141716 efficiently triggers PS exposure in both cell lines, a key "eat-me"

signal for macrophage-engulfment, thus preventing an undesirable inflammatory response.

SR141716 also exerts its cytotoxic effects in leukemia-derived cell lines across a range of doses at which only limited cell death was observed in non-proliferating freshly isolated PBMC, taken as normal cell counterpart. Thus, in view of the challenging task of identifying novel therapeutic agents that specifically work on cancer cells instead of normal cells, SR141716 may represent a promising chemotherapy molecule by itself or as a lead compound. In particular, the low toxicity against normal cells, especially in the absence of cell cycle induction, might suggest a potential therapeutic use of SR141716 as an ex vivo purging agent for autologous transplantation in hematologic malignancies [51,52].

Acknowledgement

This work was supported by an Internal Grant of the University of Salerno, Italy. This study was supported by sanofi-aventis (grant to M.B.), from the Associazione Educazione e Ricerca Medica Salernitana (ERMES, Naples).

References

[1] Bifulco M, Di Marzo V. The endocannabinoid system as a target for the development of new drugs for cancer therapy. Nat Med 2002;8:547–50.
[2] De Petrocellis L, Di Marzo V. An introduction to the endocannabinoid system: from the early to the latest concepts. Best Pract Res Clin Endocrinol Metab 2009;23:1–15.
[3] Di Marzo V. The endocannabinoid system: its general strategy of action, tools for its pharmacological manipulation and potential therapeutic exploitation. Pharmacol Res 2009;60:77–84.
[4] Bifulco M. The endocannabinoid system: from biology to therapy. Pharmacol Res 2009;60:75–6.
[5] Bifulco M, Laezza C, Pisanti S, Gazzerro P. Cannabinoids and cancer: pros and cons of an antitumour strategy. Br J Pharmacol 2006;148:123–35.
[6] Pisanti S, Malfitano AM, Grimaldi C, Santoro A, Gazzerro P, Laezza C, et al. Use of cannabinoid receptor agonists in cancer therapy as palliative and curative agents. Best Pract Res Clin Endocrinol Metab 2009;23:117–31.
[7] Bifulco M, Laezza C, Valenti M, Ligresti A, Portella G, DI Marzo V. A new strategy to block tumor growth by inhibiting endocannabinoid inactivation. FASEB J 2004;18:1606–8.
[8] Ligresti A, Moriello AS, Starowicz K, Matias I, Pisanti S, De Petrocellis L, et al. Antitumor activity of plant cannabinoids with emphasis on the effect of cannabidiol on human breast carcinoma. J Pharmacol Exp Ther 2006;318:1375–87.
[9] Grimaldi C, Pisanti S, Laezza C, Malfitano AM, Santoro A, Vitale M, et al. Anandamide inhibits adhesion and migration of breast cancer cells. Exp Cell Res 2006;312:363–73.
[10] Portella G, Laezza C, Laccetti P, De Petrocellis L, Di Marzo V, Bifulco M. Inhibitory effects of cannabinoid CB1 receptor stimulation on tumor growth and metastatic spreading: actions on signals involved in angiogenesis and metastasis. FASEB J 2003;17:1771–3.
[11] Pisanti S, Borselli C, Oliviero O, Laezza C, Gazzerro P, Bifulco M. Antiangiogenic activity of the endocannabinoid anandamide. Correlation to its tumour-suppressor efficacy. J Cell Physiol 2007;211:495–503.
[12] Bifulco M, Gazzerro P, Laezza C, Pentimalli F. Endocannabinoids as emerging suppressors of angiogenesis and tumor invasion. Oncol Rep 2007;17:813–6.
[13] Laezza C, Pisanti S, Malfitano AM, Bifulco M. The anandamide analog, Met-F-AEA, controls human breast cancer cell migration via the RHOA/RHO kinase signalling pathway. Endocr Relat Cancer 2008;15:965–74.
[14] McKallip RJ, Lombard C, Fisher M, Martin BR, Ryu S, Grant S, et al. Targeting CB2 cannabinoid receptors as a novel therapy to treat malignant lymphoblastic disease. Blood 2002;100:627–34.
[15] Maccarrone M, Lorenzon T, Bari M, Melino G, Finazzi-Agro A. Anandamide induces apoptosis in human cells via vanilloid receptors. Evidence for a protective role of cannabinoid receptors. J Biol Chem 2000;275:31938–45.
[16] Sarker KP, Maruyama I. Anandamide induces cell death independently of cannabinoid receptors or vanilloid receptor 1: possible involvement of lipid rafts. Cell Mol Life Sci 2003;60:1200–8.
[17] Rinaldi-Carmona M, Barth F, Healume M, Shire D, Calandra B, Congy C, et al. SR141716A, a potent and selective antagonist of the brain cannabinoid receptor. FEBS Lett 1994;350:240–4.
[18] Sarnataro D, Pisanti S, Santoro A, Gazzerro P, Malfitano AM, Laezza C, et al. The cannabinoid CB1 receptor antagonist rimonabant (SR141716) inhibits human breast cancer cell proliferation through a lipid raft-mediated mechanism. Mol Pharmacol 2007;70:1298–306.
[19] Malfitano AM, Laezza C, Pisanti S, Gazzerro P, Bifulco M. Rimonabant (SR141716) exerts anti-proliferative and immunomodulatory effects in human peripheral blood mononuclear cells. Br J Pharmacol 2008;153:1003–10.
[20] Flygare J, Gustafsson K, Kimby E, Christensson B, Sander B. Cannabinoid receptor ligands mediate growth inhibition and cell death in mantle cell lymphoma. FEBS Lett 2005;579:6885–9.
[21] Gazzerro P, Malfitano AM, Proto MC, Santoro A, Pisanti S, Caruso MG, et al. Synergistic inhibition of human colon cancer cell growth by the cannabinoid CB1 receptor antagonist rimonabant and oxaliplatin. Oncol Rep 2010;23:171–5.
[22] Bifulco M, Santoro A, Laezza C, Malfitano AM. Cannabinoid receptor CB1 antagonists state of the art and challenges. Vitam Horm 2009;81:159–89.
[23] Nicoletti I, Migliorati G, Pagliacci MC, Grignani F, Riccardi C. A rapid and simple method for measuring thymocyte apoptosis by propidium iodide staining and flow cytometry. J Immunol Methods 1991;139:271–9.
[24] Scaduto Jr RC, Grotyohann LW. Measurement of mitochondrial membrane potential using fluorescent rhodamine derivatives. Biophys J 1999;76:469–77.
[25] Rothe G, Valet G. Flow cytometric analysis of respiratory burst activity in phagocytes with hydroethidine and 2′,7′-dichlorofluorescin. J Leukoc Biol 1990;47:440–8.
[26] Gogvadze V, Orrenius S, Zhivotovsky B. Mitochondria as targets for chemotherapy. Apoptosis 2009;14:624–40.
[27] Scorrano L, Oakes SA, Opferman JT, Cheng EH, Sorcinelli MD, Pozzan T, et al. BAX and BAK regulation of endoplasmic reticulum Ca^{2+}: a control point for apoptosis. Science 2003;300:135–9.
[28] Li M, Kondo T, Zhao QL, Li FJ, Tanabe K, Arai Y, et al. Apoptosis induced by cadmium in human lymphoma U937 cells through Ca2+-calpain and caspase-mitochondria-dependent pathways. J Biol Chem 2000;275:39702–9.
[29] Arai Y, Kondo T, Tanabe K, Zhao QL, Li FJ, Ogawa R, et al. Enhancement of hyperthermia-induced apoptosis by local anesthetics on human histiocytic lymphoma U937 cells. J Biol Chem 2002;277:18986–93.
[30] Kroemer G, Galluzzi L, Brenner C. Mitochondrial membrane permeabilization in cell death. Physiol Rev 2007;87:99–163.
[31] Cao G, Xing J, Xiao X, Liou AK, Gao Y, Yin XM, et al. Critical role of calpain I in mitochondrial release of apoptosis-inducing factor in ischemic neuronal injury. J Neurosci 2007;27:9278–93.
[32] Vandenabeele P, Vanden Berghe T, Festjens N. Caspase inhibitors promote alternative cell death pathways. Sci STKE 2006;2006:pe44.
[33] Yu SW, Andrabi SA, Wang H, Kim NS, Poirier GG, Dawson TM, et al. Apoptosis-inducing factor mediates poly(ADPribose) (PAR) polymer-induced cell death. Proc Natl Acad Sci USA 2006;103:18314–9.
[34] Hassa PO. The molecular "Jekyll and Hyde" duality of PARP1 in cell death and cell survival. Front Biosci 2009;14:72–111.
[35] Imre G, Dunai Z, Petak I, Mihalik R. Cystein cathepsin and Hsp90 activities determine the balance between apoptotic and necrotic cell death pathways in caspase-compromised U937 cells. Biochim Biophys Acta 2007;1773:1546–57.
[36] Chaitanya GV, Babu PP. Differential PARP cleavage: an indication of heterogeneous forms of cell death and involvement of multiple proteases in the infarct of focal cerebral ischemia in rat. Cell Mol Neurobiol 2009;29:563–73.
[37] Yu HG, Ai YW, Yu LL, Zhou XD, Liu J, Li JH, et al. Phosphoinositide 3-kinase/AKT pathway plays an important role in chemoresistance of gastric cancer cells against etoposide and doxorubicin induced cell death. Int J Cancer 2008;122:433–43.
[38] Oh JH, Lee TJ, Kim SH, Choi YH, Lee SH, Lee JM, et al. Induction of apoptosis by withaferin A in human leukemia U937 cells through down-regulation of AKT phosphorylation. Apoptosis 2008;13:1494–504.
[39] de Frias M, Iglesias-Serret D, Cosialls AM, Coll-Mulet L, Santidrián AF, González-Gironès DM, et al. AKT inhibitors induce apoptosis in chronic lymphocytic leukemia cells. Haematologica 2009;94:1698–707.
[40] Eapen AK, Henry MK, Quelle DE, Quelle FW. DNA damage-induced G(1) arrest in hematopoietic cells is overridden following phosphatidylinositol 3-kinase-dependent activation of cyclin-dependent kinase 2. Mol Cell Biol 2001;21:6113–21.
[41] Yu C, Mao X, Li WX. Inhibition of the PI3K pathway sensitizes fludarabine-induced apoptosis in human leukemic cells through an inactivation of MAPK-dependent pathway. Biochem Biophys Res Commun 2005;331:391–7.
[42] Powles T, te Poele R, Shamash J, Chaplin T, Propper D, Joel S, et al. Cannabis-induced cytotoxicity in leukemic cell lines: the role of the cannabinoid receptors and the MAPK pathway. Blood 2005 Feb 1;105(3):1214–21.
[43] Jaattela M, Tschopp J. Caspase-independent cell death in T lymphocytes. Nat Immunol 2003;4:416–23.
[44] Kroemer G, Galluzzi L, Vandenabeele P, Abrams J, Alnemri ES, Baehrecke EH, et al. Classification of cell death: recommendations of the Nomenclature Committee on Cell Death 2009. Cell Death Differ 2009;16:3–11.
[45] Athanasiou A, Smith PA, Vakilpour S, Kumaran NM, Turner AE, Bagiokou D, et al. Vanilloid receptor agonists and antagonists are mitochondrial inhibitors: how vanilloids cause non-vanilloid receptor mediated cell death. Biochem Biophys Res Commun 2007;354:50–5.
[46] Athanasiou A, Clarke AB, Turner AE, Kumaran NM, Vakilpour S, Smith PA, et al. Cannabinoid receptor agonists are mitochondrial inhibitors: a unified hypothesis of how cannabinoids modulate mitochondrial function and induce cell death. Biochem Biophys Res Commun 2007;364:131–7.
[47] Boujrad H, Gubkina O, Robert N, Krantic S, Susin SA. AIF-mediated programmed necrosis: a highly regulated way to die. Cell Cycle 2007;6:2612–9.

[48] Wang Y, Dawson VL, Dawson TM. Poly(ADP-ribose) signals to mitochondrial AIF: a key event in parthanatos. Exp Neurol 2009;218:193–202.
[49] Wang Y, Kim NS, Li X, Greer PA, Koehler RC, Dawson VL, et al. Calpain activation is not required for AIF translocation in PARP-1-dependent cell death (parthanatos). J Neurochem 2009;110:687–96.
[50] Heeres PT, Hergenrother PJ. Poly(ADP-ribose) makes a date with death. Curr Opin Chem Biol 2007;11:644–53.
[51] Lee NS, Cheong HJ, Kim SJ, Kim SE, Kim CK, Lee KT, et al. Ex vivo purging of leukemia cells using tumor-necrosis-factor-related apoptosis-inducing ligand in hematopoietic stem cell transplantation. Leukemia 2003;17:1375–83.
[52] Kornacker M, Stumm J, Pott C, Dietrich S, Süssmilch S, Hensel M, et al. Characteristics of relapse after autologous stem-cell transplantation for follicular lymphoma: a long-term follow-up. Ann Oncol 2009;20:722–8.